Letter Vol. 50, No. 17/1 September 2025/Optics Letters 5478



Resolution enhancement in evanescent light illumination microscopy using microsphere lenses

Songlin Yang,[1,*] Jia Yang,[1] Ran Ye,[1,2] Yurong Cao,[1] and Yong-Hong Ye[1,3]

[1] School of Computer and Electronic Information, Nanjing Normal University, Nanjing 210023, China
[2] ran.ye@njnu.edu.cn
[3] yeyonghong@njnu.edu.cn
*slyang@njnu.edu.cn

Received 29 May 2025; revised 16 July 2025; accepted 14 August 2025; posted 15 August 2025; published 28 August 2025

Weakly scattering samples such as low-refractive-index nanomaterials present significant challenges in super-resolution imaging, because their weak scattering signals are difficult to distinguish from background noise. Here, we propose microsphere-enhanced evanescent light illumination microscopy (MS-EIM) for the label-free super-resolution imaging of weakly scattering samples. We used the MS-EIM method to perform simulated imaging of transparent samples with a 100-nm gap to investigate its imaging performance. Subsequently, the feasibility of MS-EIM for super-resolution imaging of weakly scattering samples was experimentally validated. This MS-EIM is a wide-field, real-time imaging technique with potential applications in the field of high-speed, label-free biomedical imaging. © 2025 Optica Publishing Group. All rights, including for text and data mining (TDM), Artificial Intelligence (AI) training, and similar technologies, are reserved.

https://doi.org/10.1364/OL.569320

Recognizing the optical signal of a target sample and effectively separating it from the surrounding background is a critical step in optical detection and imaging, and the three challenges associated with it are resolution, specificity, and sensitivity. In principle, the presence of any object should scatter incident photons, thereby enabling its detection under conditions where the detection and imaging methods are sufficiently sensitive. However, the intensity of the scattered light is directly proportional to the square of the object's size, and the magnitude of the scattered signal experiences a substantial decline as the sample size diminishes. Furthermore, the noise originating from both the background light and the instrument interferes with the feeble scattering signals emitted by nanosamples. This interference presents significant challenges to the detection and imaging of nanosamples, particularly those with low refractive indices. Therefore, specialized methods grounded in physical and chemical theories are necessary to endow the instrument with the capability of detecting weakly scattering signals of the target sample in the presence of complex background signals. For instance, through fluorescent labeling of the target molecule, the specificity of its scattering signal can be enhanced, thereby facilitating the discrimination of the signal from the background noise. The emission spectrum is then separated from the excitation spectrum, allowing detection and imaging at the single molecule level. Furthermore, it is possible to achieve resolution that exceeds the diffraction limit by employing methods such as stimulated emission depletion (STED) [1], stochastic optical reconstruction microscopy (STORM) [2], and photoactivated localization microscopy (PALM) [3].

In contrast to the limitations of fluorescence imaging, photons generated by the elastic scattering of nanoobjects are not restricted by light saturation. To achieve the desired flux of scattered photons, it is only necessary to increase the power of the illuminating light. However, the detection of scattering light from extremely small nanoobjects is typically constrained by the ultra-weak nature of the scattering light. This ultra-weak scattering light is highly vulnerable to interference from background signals, thereby presenting a significant challenge for the high signal-to-noise ratio (SNR) detection and imaging. The optimization of the SNR is contingent on the maximization of the signal and the minimization of the background signal. The former can be realized by means of interferometric detection, since the amplitude of the interferometric term in the scattered field distribution of a nano-object is linearly related to the size of the object. The interferometric scattering (iSCAT) microscopy technique has demonstrated its efficacy and advantages in detecting extremely weak scattering signals [4,5]. The most successful methods for the latter are dark-field microscopy (DFM) [6] and total internal reflection microscopy (TIRM). DFM improves imaging sensitivity by suppressing background light and enhancing contrast between tiny objects and the background. TIRM illuminates the sample with evanescent light, which can be generated by a prism, an objective lens [7], or a waveguide [8,9]. The exponential attenuation of evanescent light in the direction of the vertical interface results in the confinement of this light to the near-field region. Consequently, the most significant contribution of evanescent light illumination is its ability to effectively separate the illumination and imaging optical paths. This separation minimizes the background signal and facilitates the detection of the scattering signal from the sample by the optical microscope, thereby increasing the sensitivity. TIRM has been shown to enable the detection and imaging of single proteins on a plain glass surface by imaging the interference between the evanescent lights scattered by the single proteins and by the natural roughness of the cover glass

[10]. However, TIRM with a resolution beyond the diffraction limit still relies on other methods, such as STED [11], structured illumination [12–14], rotating coherent illumination [15], random illumination [7], spatial frequency shift [16], and polarized scattering [17].

In 2011, a novel technique was developed to enhance the imaging resolution of optical microscopes through microsphere lenses [18]. In the past decade, microsphere-assisted microscopy has been integrated with several imaging techniques to enhance the lateral resolution of integrated imaging systems, including scanning laser confocal microscopy [19–21], quantitative phase microscopy [22–25], atomic force microscopy [26], hyperspectral microscopy [27,28], Raman spectroscopy [29,30], polarized light microscopy [31], and others. The resolution of microsphere-assisted microscopy has been reported to be linked to photonic nanojets [20,32], numerical aperture [33], evanescent waves [34,35], virtual image theory [36,37], and others [38,39]. However, it is important to note that the material characteristics of the sample can also exert a considerable influence on this resolution. So far, several methods, including dark-field imaging [40] and the use of optical substrates [41], have enabled microsphere-assisted microscopy for super-resolution imaging of weakly scattering samples with low refractive indices. In contrast, evanescent light illumination can provide a simple and effective method for microsphere-assisted microscopy to improve the imaging resolution of weakly scattering samples. This is attributable to the fact that evanescent light illumination possesses a dark background that surpasses that of DFM, which can significantly improve the imaging contrast of weakly scattering samples. In addition, the approach of improving imaging quality through illumination optimization is the least harmful to the sample. In turn, microsphere lenses enhance the lateral resolution of evanescent light illumination microscopy, thus forming a complementary relationship between the two techniques.

Here, we developed an imaging technique called microsphere-enhanced evanescent light illumination microscopy (MS-EIM), which achieves high-quality, label-free, super-resolution imaging of weakly scattering samples. This imaging technique first uses evanescent light illumination to suppress background noise, thereby enhancing the imaging contrast of weakly scattering samples. It then uses a microsphere lens to break through the Abbe diffraction limit and achieve super-resolution imaging of the weakly scattering samples. We performed this technique on transparent samples to demonstrate its superior performance over conventional microsphere-assisted microscopy and evanescent light illumination microscopy (EIM).

In an MS-EIM, the microsphere collects two parts of the scattered light signal. The first part comes from the sample, which comprises low-frequency propagating waves that delineate the sample profile, as well as high-frequency evanescent waves that characterize the fine structure. The second part is derived from the illumination process, which is generated by the microspheres coupling the evanescent illumination light and converting it into propagating light. The background signal produced by the latter is evidently not beneficial for improving image resolution. Rather, it serves to obscure the scattering signal of the sample, resulting in a deterioration of imaging quality. Therefore, suppression of evanescent light used for illumination coupled by microspheres is crucial for MS-EIM. A reasonable increase in the working distance of the microspheres can reduce the effect

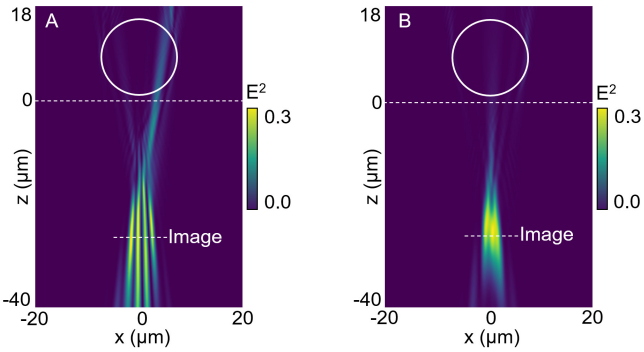


Fig. 1. (A), (B) The images of four adjacent PS nanoparticle samples with a gap of 100 nm obtained using MS-EIM and conventional microsphere-assisted microscopy, respectively.

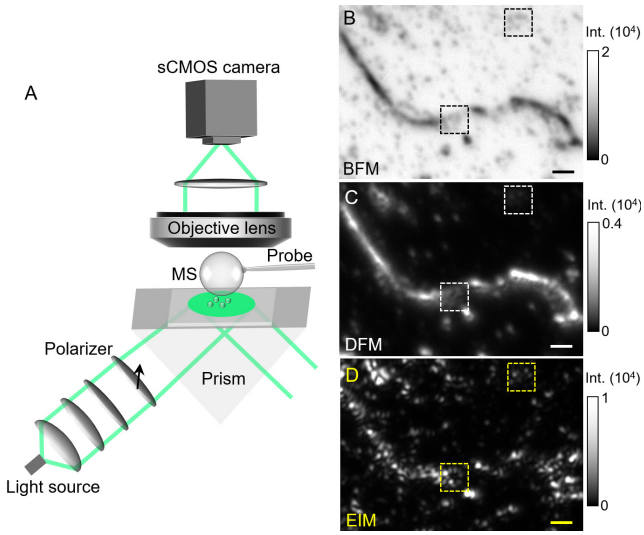


Fig. 2. (A) Schematic of the MS-EIM experimental setup. (B)–(D) The diffraction-limited images of PS nanoparticles with a diameter of 100 nm using BFM, DFM, and EIM, respectively. Scale bar: 2 μm.

of microsphere-evanescent light coupling on imaging performance (see Fig. S2 in Supplement 1). To validate the MS-EIM, we simulate the imaging of four equally spaced polystyrene (PS) nanoparticle samples. Figures 1(A) and 1(B) show the images of adjacent PS nanoparticle samples with a gap of 100 nm obtained using MS-EIM and microsphere-assisted microscopy, respectively. As shown in the figure, the PS sample cannot be resolved using microsphere-assisted microscopy. However, it can be resolved by MS-EIM.

The MS-EIM setup is constructed using a Leica DM 2500M upright optical microscope (see Fig. 2(A)). We excite evanescent light by directing collimated, incoherent light with a wavelength of 510 nm at an incident angle of about 60°. This angle is larger than the critical angle of about 41° at the BK7 optical glass–air interface. The sample to be observed is located on the surface of a BK7 slide, which is in contact with a BK7 prism through a matching solution with a refractive index of 1.51. A silica microsphere with a diameter of 15 μm is affixed to the probe using a UV-curable adhesive. The probe is attached

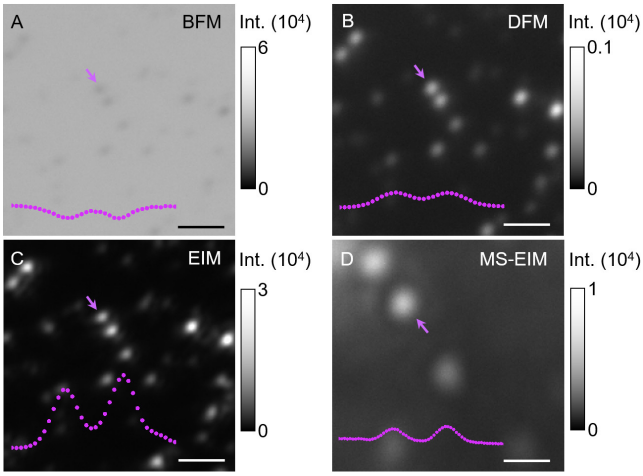


Fig. 3. (A)–(D) Images of PS nanoparticles with a diameter of 100 nm obtained by BFM, DFM, EIM, and MS-EIM, respectively. The lower left inset corresponds to the intensity profile in the direction of the arrow. Scale bar: 2 μm.

to a three-dimensional precision linear displacement stage, the function of which is to control the spatial position of the microspheres. The scattering signal from the sample is first acquired by the microspheres, then transmitted to the objective lens (Leica 100 × 0.75), and finally imaged by the objective lens into the sCMOS camera (Teledyne Photometrics Prime BSI).

To analyze the performance of EIM and DFM for imaging weakly scattering samples, we obtained diffraction-limited images of PS nanoparticles with a diameter of 100 nm. As illustrated in Figs. 2(B)–2(D), the images of PS nanoparticles were obtained using bright-field microscopy (BFM), DFM, and EIM, respectively. The BFM and DFM utilized in the experiments are built-in features of the Leica DM 2500M microscope. Both use the same objective lens (Leica 100×, 0.75) and an incoherent monochromatic light souce with a central wavelength of 540 nm. Figure 2(B) shows that the BFM captures light reflected from the planar quartz substrate, presenting a bright background. However, the scattered light from the PS nanoparticles is weaker than the reflected light from the substrate, resulting in a grayish appearance. In contrast, DFM utilizes an oblique illumination technique that effectively suppresses the substrate's reflected light entering the imaging objective. This leads to the scattered light emitted by PS nanoparticles becoming the primary contributor to the optical signal captured by the imaging objective, consequently increasing its brightness (see Fig. 2(C)). Figure 2(D) shows that the contours of PS nanoparticles obtained by EIM are more clearly defined than those obtained by DFM. In addition, the dashed box-marked region also shows that adjacent PS nanoparticles cannot be resolved by BFM and DFM, but can be resolved by EIM. Figure 2 reveals the higher contrast and resolution of EIM compared to DFM when imaging weakly scattering samples.

To investigate the effect of microspheres on EIM, we integrated 15-μm-diameter silica microspheres into a prism-based TIRM to form MS-EIM. First, PS nanoparticles with a diameter of 100 nm were used as samples to evaluate the performance of the MS-EIM. As shown in Figs. 3(A)–3(D), the images of PS nanoparticles were obtained using a variety of imaging systems, including BFM, DFM, EIM, and MS-EIM, respectively. To evaluate the quality of these images, we calculated the contrast and valley-to-peak ratio (VPR) using the lower-left insets in Figs. 3(A)–3(D), yielding values of −0.05, 0.63, 0.93, 0.53 for contrast and 0.52, 0.54, 0.31, 0.10 for VPR, respectively (see Fig. S4 in Supplement 1). The data demonstrate that images obtained by EIM exhibit optimal contrast, while those acquired by BFM show inferior contrast. Additionally, the data indicate that the contrast of images obtained via MS-EIM is comparable to that of DFM but inferior to that of EIM. Microspheres increase the NA of the imaging system, thereby enlarging the aperture angle over which the objective lens collects light. However, they also introduce additional magnification into the system, which reduces the number of photons collected by individual pixels and consequently leads to decreased image contrast. Although the contrast of MS-EIM is not optimal, it has the best resolution in terms of the calculated VPR. The VPR further demonstrates that images of weakly scattering samples obtained by BFM have low resolution, resulting in structural details about the samples not being presented.

PS nanoparticle samples with smaller structural features were used to validate the higher lateral resolution of MS-EIM compared to DFM and EIM. The experimental results show that structures unresolved by DFM can be resolved by both EIM and MS-EIM, with MS-EIM achieving higher resolution. Additionally, the images of nanoparticles exhibit broadening perpendicular to the propagation direction of the evanescent light, which may be attributed to the anisotropic resolution in EIM (see Fig. S5 in Supplement 1). The resolution of an imaging system can be determined by fitting a Gaussian function to the image intensity profile of a point-like object that is smaller than the theoretical resolution, and then measuring the full width at half maximum (FWHM). Here, 100-nm diameter PS nanoparticles served as point sources for resolution analysis. Images of isolated nanoparticles obtained via MS-BFM, MS-DFM, and MS-EIM are presented in Figs. 4(A)–4(C). Line profiles across the selected nanoparticle (purple arrows) are shown in Figs. 4(D)–4(F). Gaussian fitting yielded FWHM values of 180 nm, 234 nm, and 135 nm for MS-BFM, MS-DFM, and MS-EIM, respectively. These results demonstrate that for unlabeled transparent samples, integrating microspheres with BFM enables lateral super-resolution but reduces image contrast. In DFM with reflected illumination, large microspheres strongly scatter light, degrading image quality. In contrast, EIM reduces background light and avoids intense scattering, ensuring microspheres maintain high lateral resolution for transparent samples.

In summary, we demonstrated microsphere-enhanced evanescent light illumination microscopy (MS-EIM). The MS-EIM incorporates two key concepts to achieve super-resolution imaging of samples that exhibit weak scattering properties. The first concept involves the suppression of background light generation through evanescent wave illumination, which effectively reduces the influence of background light and noise on the scattered signal from the sample, thereby enhancing the imaging contrast for weakly scattering specimens. The second concept involves the coupling of the evanescent wave, which contains detailed structural information about the sample, through a microsphere lens. This process converts the evanescent wave into a propagating wave that can be detected by the objective lens, thereby overcoming the diffraction limit and facilitating super-resolution imaging of weakly scattering samples. The simulated and experimental

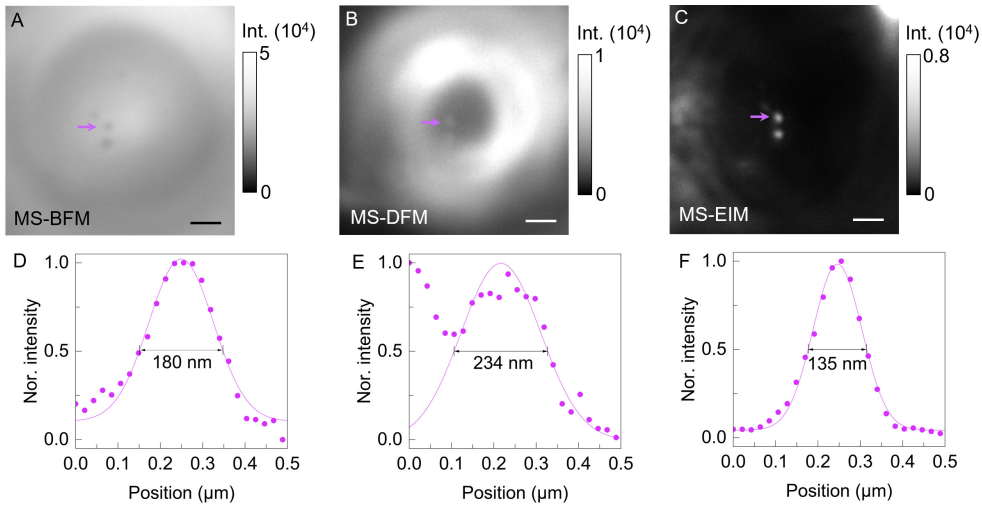


Fig. 4. (A)–(C) Images of PS nanoparticles with a diameter of 100 nm obtained by MS-BFM, MS-DFM, and MS-EIM, respectively. (D)–(F) Distribution of gray values corresponding to the arrow directions in (A)–(C). Scale bar: 2 μm.

results demonstrated that the imaging resolution of MS-EIM surpasses that of bright-field and dark-field microscopes, as well as evanescent light illumination microscopes, particularly when applied to weakly scattering samples.

Of course, the current MS-EIM still has issues that need to be improved to meet imaging requirements in complex environments, such as the resolution anisotropy caused by evanescent light illumination, the need for evanescent light with a larger lateral wavenumber to match the liquid background in biological imaging, and the improvement of imaging contrast. These will become the next research focus of MS-EIM technology. With the resolution of these issues, MS-EIM will have broader application prospects in the field of label-free super-resolution imaging.

Funding. National Natural Science Foundation of China (62375135, 62505138); the Scientific Research Starting Foundation of Nanjing Normal University (184080H201B122).

Disclosures. The authors declare no conflicts of interest.

Data availability. Data underlying the results presented in this paper are not publicly available at this time but may be obtained from the authors upon reasonable request.

Supplemental document. See Supplement 1 for supporting content.

REFERENCES

1. S. W. Hell and J. Wichmann, Opt. Lett. **19**, 780 (1994).
2. M. J. Rust, M. Bates, and X. Zhuang, Nat. Methods **3**, 793 (2006).
3. E. Betzig, G. H. Patterson, R. Sougrat, *et al.*, Science **313**, 1642 (2006).
4. P. Kukura, H. Ewers, C. Müller, *et al.*, Nat. Methods **6**, 923 (2009).
5. K. Iqbal, J. C. Thiele, E. Pfitzner, *et al.*, ACS Photonics **12**, 2647 (2025).
6. P. F. Gao, G. Lei, and C. Z. Huang, Anal. Chem. **93**, 4707 (2021).
7. K. Affannoukoué, S. Labouesse, G. Maire, *et al.*, Optica **10**, 1009 (2023).
8. D. J. Hill, C. W. Pinion, J. D. Christesen, *et al.*, ACS Photonics **1**, 725 (2014).
9. E. Glushkov, A. Archetti, A. Stroganov, *et al.*, ACS Photonics **6**, 3100 (2019).
10. P. Zhang, L. Zhou, R. Wang, *et al.*, Nat. Commun. **13**, 2298 (2022).
11. T. J. Gould, J. R. Myers, and J. Bewersdorf, Opt. Express **19**, 13351 (2011).
12. R. Fiolka, M. Beck, and A. Stemmer, Opt. Lett. **33**, 1629 (2008).
13. D. Li, L. Shao, B.-C. Chen, *et al.*, Science **349**, aab3500 (2015).
14. W. Zhao, S. Zhao, L. Li, *et al.*, Nat. Biotechnol. **40**, 606 (2022).
15. F. Jünger, P. v. Olshausen, and A. Rohrbach, Sci. Rep. **6**, 30393 (2016).
16. C. Pang, X. Liu, Q. Zhang, *et al.*, Adv. Photonics Res. **5**, 2300341 (2024).
17. C. Liu, Z. Chen, Z. Xu, *et al.*, J. Microsc. **298**, 305 (2025).
18. Z. Wang, W. Guo, L. Li, *et al.*, Nat. Commun. **2**, 218 (2011).
19. Y. Yan, L. Li, C. Feng, *et al.*, ACS Nano **8**, 1809 (2014).
20. L. Hüser, T. Pahl, S. Hagemeier, *et al.*, J. Eur. Opt. Soc. Publ. **21**, 16 (2025).
21. J. S. Moon, H. Lee, J. H. Lee, *et al.*, ACS Photonics **8**, 2642 (2021).
22. F. Wang, L. Liu, P. Yu, *et al.*, Sci. Rep. **6**, 24703 (2016).
23. I. Kassamakov, S. Lecler, A. Nolvi, *et al.*, Sci. Rep. **7**, 3683 (2017).
24. S. Perrin, Y. J. Donie, P. Montgomery, *et al.*, Phys. Rev. Appl. **13**, 014068 (2020).
25. V. Abbasian, T. Pahl, L. Hüse, *et al.*, Light: Adv. Manuf. **5**, 133 (2024).
26. Y. Hong, S. Xiao, C. Zhai, *et al.*, Opt. Express **31**, 27520 (2023).
27. M. Mollaei, P. Soltani, M. Panahi, *et al.*, Opt. Lett. **48**, 6292 (2023).
28. J. Park, Y. Choi, S. Kwon, *et al.*, Light: Sci. Appl. **13**, 122 (2024).
29. J. Kasim, Y. Ting, Y. Y. Meng, *et al.*, Opt. Express **16**, 7976 (2008).
30. X. Zheng, C. Zong, M. Xu, *et al.*, Small **11**, 3395 (2015).
31. R. Ye, X. Zhang, L. Zhi, *et al.*, Opt. Lett. **50**, 908 (2025).
32. H. Yang, R. Trouillon, G. Huszka, *et al.*, Nano Lett. **16**, 4862 (2016).
33. A. Darafsheh and V. Abbasian, Light: Sci. Appl. **12**, 22 (2023).
34. Y. Ben-Aryeh, J. Opt. Soc. Am. A **33**, 2284 (2016).
35. S. Yang, Y.-H. Ye, Q. Shi, *et al.*, J. Phys. Chem. C **124**, 25951 (2020).
36. L. Chen, Y. Zhou, Y. Li, *et al.*, Appl. Phys. Rev. **6**, 021304 (2019).
37. A. R. Bekirov, B. S. Luk'yanchuk, Z. Wang, *et al.*, Opt. Mater. Express **11**, 3646 (2021).
38. Y. Duan, G. Barbastathis, and B. Zhang, Opt. Lett. **38**, 2988 (2013).
39. A. V. Maslov and V. N. Astratov, Appl. Phys. Lett. **110**, 261107 (2017).
40. S. Perrin, H. Li, K. Badu, *et al.*, Phys. Status Solidi-Rapid Res. Lett. **13**, 1800445 (2018).
41. S. Yang, Y. Cao, Q. Shi, *et al.*, J. Phys. Chem. C **123**, 28353 (2019).